crystals

MDPI

Article

One-Step Carbothermal Synthesis of Super Nanoadsorbents for Rapid and Recyclable Wastewater Treatment

Wen-chan Ji [1,2], Ping Hu [1,2,*], Xiao-yu Wang [1], Sandra Elizabeth Saji [3], Tian Chang [1,4], Xin-yu Zhu [1,2], Fairy Fan Yang [1], Qi-gao Cao [4], Rui Dang [4], Kuai-she Wang [1,2] and Zongyou Yin [3,*]

1 School of Metallurgy Engineering, Xi'an University of Architecture and Technology, Xi'an 710055, China; Wenchan1996@xauat.edu.cn (W.-c.J.); Xiaoyu_W@xauat.edu.cn (X.-y.W.); changtian1994@126.com (T.C.); 7954780@xauat.edu.cn (X.-y.Z.); yf_0416@xauat.edu.cn (F.F.Y.); wangkuaishe888@126.com (K.-s.W.)
2 National and Local Joint Engineering Research Center for Functional Materials Processing, Xi'an University of Architecture and Technology, Xi'an 710055, China
3 Research School of Chemistry, The Australian National University, Canberra, ACT 2601, Australia; sandra.poozhikunnel@anu.edu.au
4 Northwest Institute for Non-Ferrous Metal Research, Xi'an 710016, China; wang826@xauat.edu.cn (Q.-g.C.); Chenbo1998@xauat.edu.cn (R.D.)
* Correspondence: huping@xauat.edu.cn (P.H.); zongyou.yin@anu.edu.au (Z.Y.)

Abstract: As a potential magnetic super adsorbent in wastewater treatment, Fe_3O_4 has been researched intensively up to date. However, its key problem of poor comprehensive magnetic properties is still challenging. In this work, an effective solution to this problem has been developed by a one-step carbothermal synthesis of Fe_3O_4 crystals, which are merited with pure-stoichiometry (FeO-phase free), high crystallinity, small-size (~10 nm), strong magnetism and sensitive magnetic response. The unveiled saturation magnetization of Fe_3O_4 nanoparticles reaches as high as 90.32 emu·g^{-1}, and the fastest magnetic response time is as short as only 5 s. Such magnetic Fe_3O_4 super adsorbents exhibit outstanding performance when applied as an adsorbent for wastewater treatment. They can quickly and effectively adsorb methylene blue with an adsorption capacity of 62.5 mg·g^{-1}, which is much higher than that of Fe_3O_4 adsorbents prepared by other methods reported in the literature. Importantly, this capacity is refreshable after removing the adsorbed methylene blue just by ultrasonic cleaning. With such combined outstanding magnetic properties and recyclable adsorption capacity, the problems associated with the conventional adsorbent solid–liquid separation could be resolved, thus making a forward development towards industrial wastewater treatment.

Keywords: magnetism; Fe_3O_4 nanoparticles; accurate fabrication; magnetic responsiveness; adsorption

Citation: Ji, W.-c.; Hu, P.; Wang, X.-y.; Saji, S.E.; Chang, T.; Zhu, X.-y.; Yang, F.F.; Cao, Q.-g.; Dang, R.; Wang, K.-s.; et al. One-Step Carbothermal Synthesis of Super Nanoadsorbents for Rapid and Recyclable Wastewater Treatment. *Crystals* **2021**, *11*, 75. https://doi.org/10.3390/cryst11010075

Received: 29 November 2020
Accepted: 13 January 2021
Published: 18 January 2021

1. Introduction

As an important functional magnetic material, Fe_3O_4 has an inverse cubic spinel structure (two Fe^{3+} with one Fe^{2+}) in which oxygen atoms form an fcc close-packed structure [1–4]. In recent years, Fe_3O_4 nanoparticles have been used as adsorbents for wastewater purification and have gradually attracted great attention from scholars at home and abroad, due to their stable physical and chemical properties, strong magnetism, large specific surface area, and ease of dispersion [5–12].

With the development of industrial technology, water pollution is currently one of the most serious environmental problems, causing potential harm to the health of humans and other organisms [13–15]. Especially, dye waste treatment in industrial wastewater has become one of the biggest challenges due to its high organic content, complex composition, deep color and contribution to large changes in water quality [16–18]. With the wastewater treatment techniques constantly innovating, various methods such as electrochemical and catalytic degradation [19], membrane filtration, adsorption, and biological treatment have come into play [20–24]. According to reports, adsorption is recognized as the most

effective method for the decolorization of printing and dyeing wastewater. Among many adsorbents that have been used in wastewater decolorization (such as activated carbon, kaolin, bagasse charcoal, and biochar), Fe_3O_4 has attracted widespread attention, due to its low price and ease of separation of solid and liquid dye components. Therefore, it has an important environmental significance that calls for the development of a cost-effective magnetic Fe_3O_4 adsorbent for removing methylene blue from waste liquid.

In this work, aiming at reusable magnetic adsorbents for efficient wastewater treatment, a solution to the key problem of poor magnetic responsiveness of Fe_3O_4 is developed by synthesizing purely-stoichiometric, monodisperse, and small-sized crystals using a one-step carbothermal strategy. Based on the original one-step reduction method [25,26], in this experiment, the carbon source is provided by adding an appropriate amount of citric acid during the sol-gel process. Some parameters, such as the amount of ferric nitrate and citric acid in the sol-gel process, reduction temperature, holding time as well as the ratio of dry gel and picric acid, have been explored and optimized to accurately control the preparation of Fe_3O_4 nanoparticles. This work uses methylene blue (MB) solution to simulate wastewater, and conducts a series of adsorption experiments using Fe_3O_4 nanoparticles as the MB adsorbent. The amount of adsorbent, reaction time, and initial concentration of MB on the adsorption performance of the material were explored. The purpose of this study is to prepare Fe_3O_4 nanoparticles by a one-step carbothermal reduction method with high magnetic properties and excellent magnetic response, that can effectively remove MB from aqueous solution with excellent recyclability. This study paves an avenue to manufacture Fe_3O_4 nanoparticles towards industrial dye wastewater treatment.

2. Materials and Methods

2.1. Synthesis of Fe_3O_4 Nanoparticles

The dry gel is prepared by the citric acid sol-gel method. Herein, the organic fuel citric acid $C_6H_8O_7{\cdot}H_2O$ is used as the carbon source, and the soluble metal salt $Fe(NO_3){\cdot}9H_2O$ is used as the iron source, which were dissolved in deionized water according to a certain molar ratio. After stirring, the solvent was evaporated and the pH adjusted to form a red-brown gel. The resulting viscous solution was poured into a glass, and dried at 100 °C in an oven, to achieve complete dehydration, which was later ground into a powder. The $C_6H_8O_7{\cdot}H_2O$-Fe $(NO_3){\cdot}9H_2O$ xerogel and picric acid were put into an autoclave at a ratio of 12:1 with sealing under an argon atmosphere, and then a carbothermal reduction reaction was conducted. In this process, picric acid explosion not only results in dispersed particles with reduced particle size, but also the CO produced could be used as a reducing agent. Through changing the three process parameters of reduction temperature, holding time, and the ratio of dry gel and picric acid in the carbothermic reduction process, the controllable preparation of single-phase nano Fe_3O_4 particles at 450–650 °C was finally realized.

2.2. Adsorption Experiment

An aqueous stock solution of MB (1000 $mg{\cdot}L^{-1}$) was prepared by dissolving MB in deionized water. Then MB aqueous solutions of different concentrations (40, 60, 80, and 100 $mg{\cdot}L^{-1}$) were prepared by successive dilution of the stock solution with deionized water. 50 mL each of MB dye solutions of different concentrations were taken and 40 mg Fe_3O_4 adsorbent was added to it. Then the solutions were shaken sufficiently in a neutral environment with a temperature of 20 °C and a pH of 7. At different time intervals, 5 mL of suspension samples were taken for external magnetic separation, and the supernatant was collected to measure its absorbance at the maximum absorption wavelength of MB at 664 nm by UV-Vis spectrophotometry, following which the adsorption capacity was calculated using the formulae [7,10]

$$A = KCL, \quad (1)$$

$$Q = [(C_0 - C_e)\, V/W] \times 100\%, \quad (2)$$

$$E = [(C_0 - C_e)/C_0] \times 100\%, \quad (3)$$

where A is the absorbance, K is the absorption coefficient of the sample, C is the concentration of the sample to be tested, L is the length of the sample in the optical path, Q is the absorption capacity of the material for MB, E is the removal rate, and C_0 is the initial dye concentration (mg/L), C_e is the equilibrium concentration of the dye in the reaction equilibrium, V is the volume of the reaction solution, and W is the weight of the adsorbent (g).

2.3. Samples Characterization

The phase structure of the samples 1–6 was studied using XRD patterns. Jade software was used to fit the strongest FeO and Fe_3O_4 diffraction peaks for semi-quantitative analysis to obtain the mass fraction of each component. FESEM (field-emission scanning electron microscope) was used to observe the surface morphology and particle size of the samples 1–5 to study the influence of different content of FeO on the shape and size of the product. Transmission electron microscopy (TEM) was used to characterize the morphology of the Fe_3O_4 (S6) nanoparticles. The room temperature magnetic hysteresis (M-H) loops of samples 1–6 were measured using a vibrating sample magnetometer (VSM) system with a maximum magnetic field of 20,000 Oe. The pure phase Fe_3O_4 (S6) was used for the adsorption experiment, and the absorbance of the solution to be tested was measured with an ultraviolet-visible spectrophotometer.

3. Results and Discussion

3.1. Characterizations of Fe_3O_4/FeO and Fe_3O_4 Nanoparticles

For convenience, the amount of xerogel and picric acid were fixed, and the ratio of ferric nitrate to citric acid was varied in the following discussion. In Figure 1a, when the molar ratio of ferric nitrate to citric acid is 1:0.5 mol, an obvious peak of FeO in samples S1–S3 is present, and that of Fe_3O_4 becomes weak, indicating that the content of Fe_3O_4 in the product diminishes.

When the molar ratio of ferric nitrate to citric acid is 1:0.8 mol, it can be observed that the main phase of samples S4 and S5 is Fe_3O_4, with a trace amount of FeO. On this basis, without changing the ratio of raw materials, the FeO content is reduced by adjusting the temperature. When the reaction temperature reaches 650 °C, there is only a single phase of Fe_3O_4 in the product without other peaks (Figure 1c). The strong and sharp diffraction peaks indicate that the sample has good crystallinity. The XRD pattern can be matched to the series of Bragg reflections corresponding to the standard phase of the spinel structure of Fe_3O_4. Six peaks at 30.16°, 35.49°, 43.01°, 53.78°, 57.21°, and 62.73° can be indexed as (220), (311), (400), (422), (511), and (440) of the cubic structure of Fe_3O_4 nanoparticles.

According to the related reports of cited literature and experimental results, the precursor formed by ferric nitrate and citric acid sol-gel is first reduced to Fe_2O_3 during the carbothermal reduction stage. The remaining free -C- in the precursor further reduces Fe_2O_3 to form Fe_3O_4. When the free -C- in the system is in excess, FeO will be gradually formed. However, it can be seen from Figure 1 that when the molar amount of citric acid is reduced from 0.8 mol to 0.5 mol, the product contains a large amount of FeO. This may be due to the fact that in the process of preparing the precursor, a longer drying time is required for the formation of 1.05 mol dry gel. A part of Fe_2O_3 gets reduced to Fe_3O_4 after drying in an oven at 100 °C for 24 h. In the carbothermal reduction stage, the Fe_3O_4 contained in the original xerogel is reduced to FeO.

The (311) diffraction peaks corresponding to the FeO/Fe_3O_4 mixture S1, S2, and S3 shifted to a higher 2θ (Figure 1b), indicating that at the mixing ratio of 1:0.5 ferric nitrate and citric acid, the doping of FeO content increases. Additionally, when the FeO content is large, it can be seen from the interlayer spacing of Fe_3O_4 that the Fe_3O_4 diffraction peak intensity is not sharp enough.

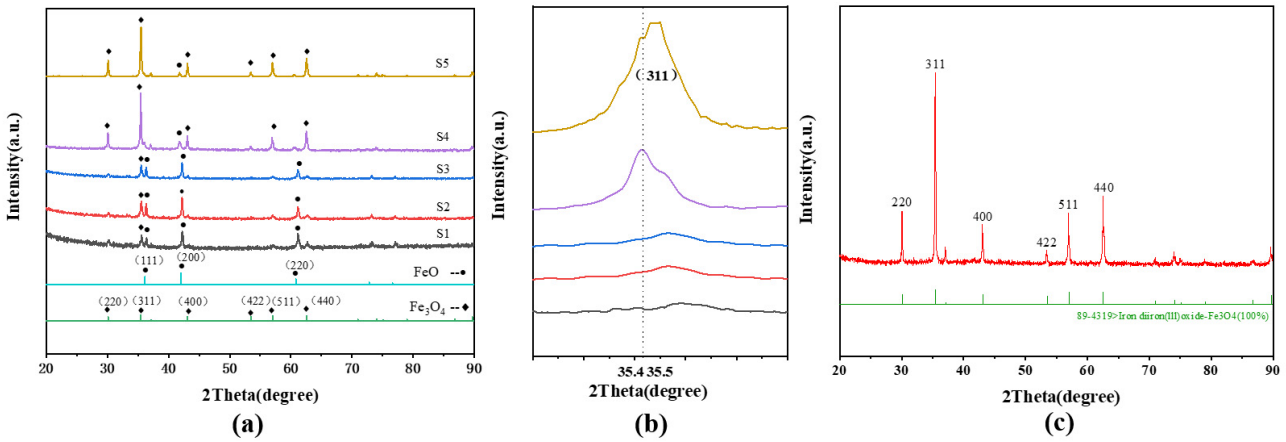

Figure 1. (**a**) XRD patterns of Fe_3O_4/FeO nanoparticles. (**b**) (311) diffraction peak of Fe_3O_4/FeO nanoparticles. (**c**) XRD pattern of Fe_3O_4 NPs (S6).

Morphological studies. Figure 2(S1–S5) shows the observed SEM images of five Fe_3O_4/FeO mixed samples. With the decrease of FeO content, the particles are obviously smaller and the size is uniform. The small spherical particles can be clearly seen from the images. The morphology of Fe_3O_4 NPs and the corresponding SAED images were obtained by high resolution transmission electron microscopy (HRTEM). Fe_3O_4 NPs (Figure 2(S6)) are spherical and uniformly sized, with a diameter of 10 nm. The HRTEM clear parts of multiple particles were selected separately, and the interplanar spacing was measured, which corresponds to the Fe_3O_4 standard card 89-4391.

It can be seen in Figure 2a that the lattice stripes of Fe_3O_4 are clear and continuous, indicating that Fe_3O_4 nanoparticles have a good crystal structure. The lattice fringe spacing of ~10 nm for Fe_3O_4 NPs is ~0.25 nm and 0.20 nm, corresponding to the (311) plane and (400) plane of the NP, respectively. The FFT of the corresponding area (Figure 2a) is displayed as a polycrystalline FFT pattern.

The difference in the crystallization process will affect the distribution of Fe^{2+} and Fe^{3+} in the octahedral sites, thereby affecting the super-exchange between Fe ions. It can be seen from XRD and TEM that the nano Fe_3O_4 particles synthesized by one-step carbothermal synthesis have high crystallinity, more than 82%, indicating the presence of fewer lattice defects. Therefore, the super-exchange between Fe-O-Fe is enhanced, and hence the magnetic properties are improved [27].

FT-IR spectra analysis. Figure 2b shows the FT-IR spectra of the obtained samples. With the decrease of FeO content in the samples, the characteristic peak of Fe_3O_4 becomes more obvious. The sample has vibration peaks at around 1620 cm^{-1} and 3400 cm^{-1}, which are attributed to the H_2O and O-H stretching vibration absorption peaks contained in the ferrite. It can be seen from the figure that the absorption vibration peak of the self-burning powder at about 570 cm^{-1} is the vibration peak of Fe_3O_4. From the enlarged FTIR image, it is observed that the characteristic peaks of the samples with more FeO content around 570 cm^{-1} have shifted to the left relative to the Fe_3O_4 samples, and the infrared absorption band gradually assumes a broad and flat form. However, the S1 and S2 samples have no characteristic peak near 550 cm^{-1}, indicating that some Fe_3O_4 is reduced to FeO excessively. This result is due to a difference in the temperatures of the carbothermal reduction reaction, which deforms the inside of the particles after heating, thereby changing the bond length, and increasing the bond frequency [27,28].

VSM analysis. The magnetic properties are summarized in Table 1. The saturation magnetization (Ms) values of the S1, S2, S3, S4, S5, and S6 (Fe_3O_4) samples are determined as 26.72, 32.69, 38.08, 70.57, 88.57, and 90.32 emu/g respectively (Figure 3a–f). It can be noticed that as the FeO content decreases, the Ms value tends to increase. The Ms value of Fe_3O_4 nanoparticles is significantly higher than that of other samples, and even higher than the Ms (86.2 emu/g) we previously reported. This result can be owed to the different

crystal sizes. From Table 1, we know that the coercivity of Fe_3O_4 nanoparticles is large, which is due to the one-step carbon thermal synthesis process. Spin barrier, spin tilt and spin glass effect due to in-situ chemical disorder on the surface of nanoparticles [25]. The following figures provide some useful information about the magnetic response of various samples. It is these magnetic properties that render potential applications in magnetic adsorbents [29,30].

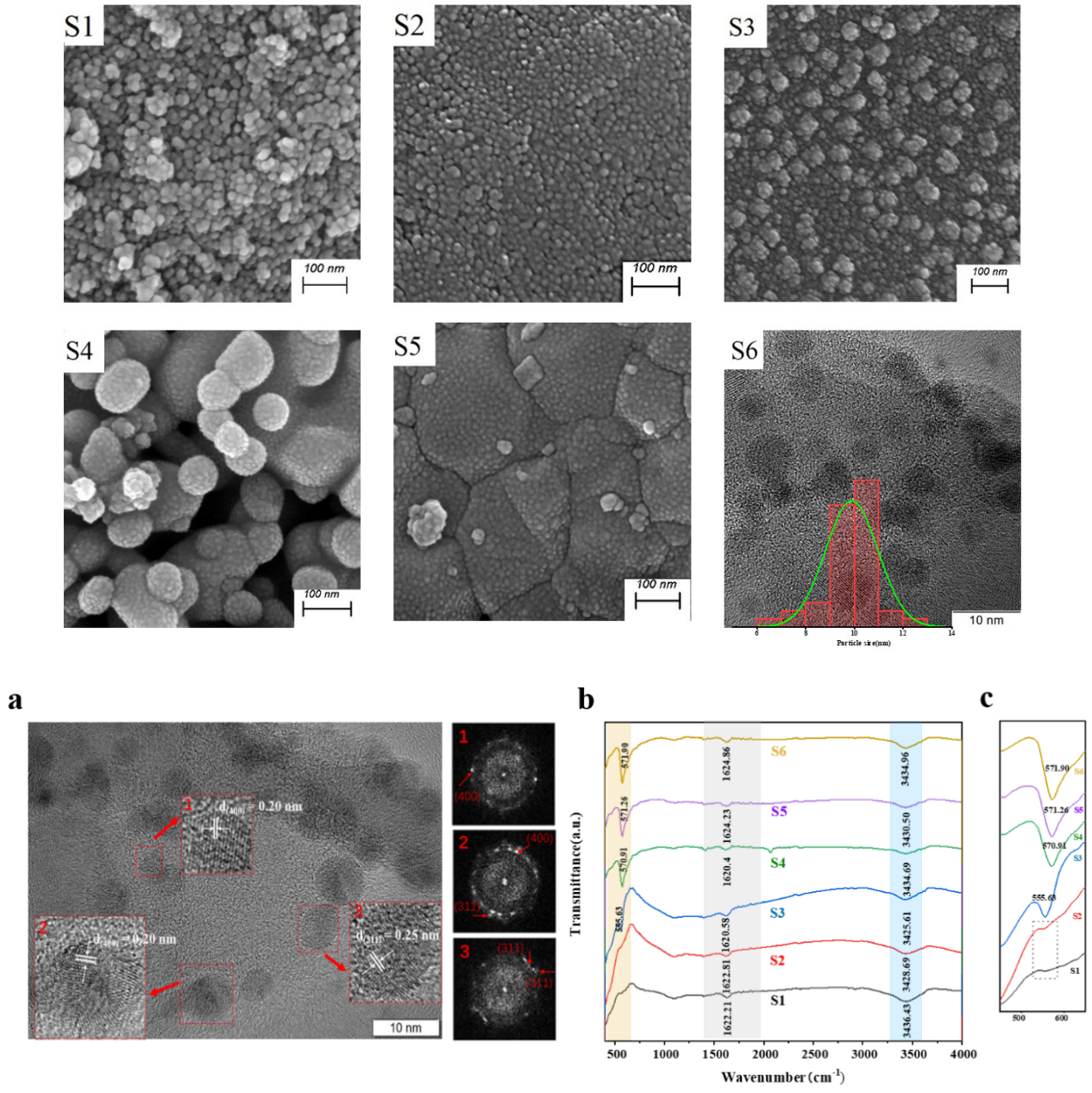

Figure 2. (**S1**–**S5**) SEM images of Fe_3O_4/FeO composites with different percentages. **S6**. TEM image of Fe_3O_4 nanoparticles and particle size distribution (in the inset). (**a**) HRTEM images of Fe_3O_4 nanoparticles and diffraction rings of Fe_3O_4 nanoparticles. (**b**) FT-IR spectra of the nanoparticles. (**c**) FT-IR spectra with an enlarged yellow area.

Table 1. Magnetic Properties of Fe_3O_4/FeO Samples.

Sample	Preparation Conditions			Fe_3O_4 (wt%)	FeO (wt%)	M_S (emu/g)	Mr (emu/g)	H_C (Oe)	
	Molar Ratio	T (°C)	T (min)					+	–
1	1:0.5	450	50	32.3	67.7	26.72	8.26	489.7	552.2
2	1:0.5	600	20	56.7	43.3	32.69	9.73	581.4	487.7
3	1:0.5	600	30	66.5	33.5	38.08	14.26	633.8	714.1
4	1:0.8	550	20	75.5	24.5	70.57	19.52	431.8	311.4
5	1:0.8	600	30	87.7	12.3	88.57	35.77	392.6	327.1
6	1:0.8	650	15	100	0	90.32	36.56	319.2	320.4

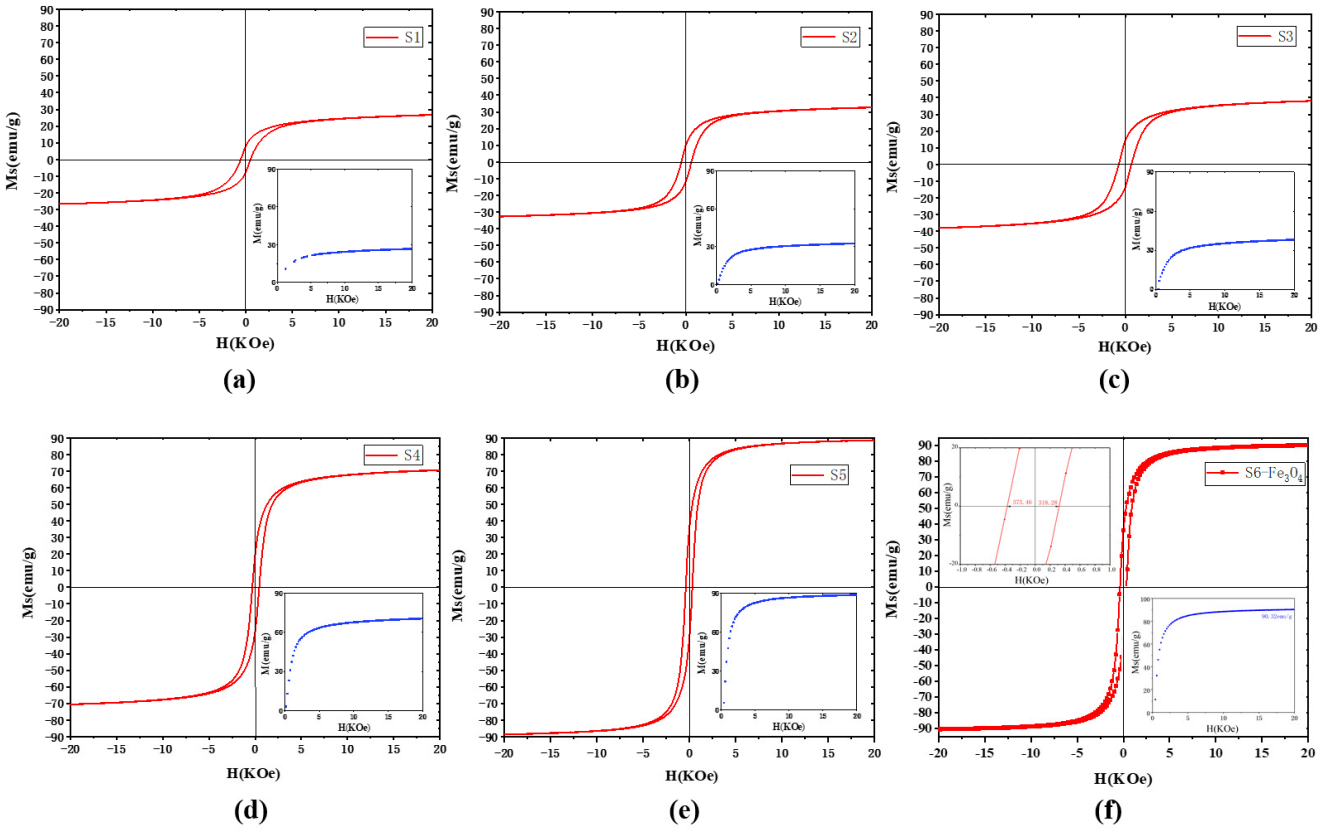

Figure 3. (**a**–**f**) Magnetization vs. magnetic field plots of S1–S6 samples at 300 K.

3.2. Magnetic Response

The samples are prone to agglomeration due to their large specific surface area and magnetic dipole interaction, which makes them difficult to be used directly. In order to study the magnetic response behavior of nanoparticles with different contents, local high temperature, high pressure, or strong shock wave generated by ultrasonic cavitation is used to greatly weaken the interaction between nanoparticles. The magnetic response tests are performed by using samples of the same quality and dissolving and dispersing them in ethanol solution under ultrasonication for 15 min. The time for which the test sample was adsorbed on the bottle wall in the magnet environment is recorded, and the same sized bottle and magnet were used to ensure comparability [31].

It can be seen from the test results (Figure 4) that samples other than S1 could be dispersed in ethanol to form a uniform suspension when there is no external magnetic field, which can be quickly assembled and separated when an external magnetic field is applied. As the FeO content in the S1 particles is higher, the particle size is larger, and FeO is insoluble in ethanol, resulting in a weaker dispersion in the ethanol solution compared

to the other four samples. Samples S4 and S5 showed a relatively faster adsorption and the solutions were clear and free of impurities. The other solutions were all turbid. As the size of the nanoparticles decreases, the turbidity of the solution increases, and the rate of adsorption by the magnet is faster. This shows that samples with higher FeO content have weaker magnetic properties and are not easily soluble in ethanol. The S6 sample is more soluble in the ethanol and is adsorbed by the magnet within 5 s. The adsorbed solution is clearer than the other five samples, indicating that the prepared Fe_3O_4 nanoparticles have high magnetic response sensitivity. Based on the rapid separation technology, the synthesized nano Fe_3O_4 particles can be used as a magnetic adsorbent to treat other pollutants such as heavy metal ions and colored dyes in wastewater.

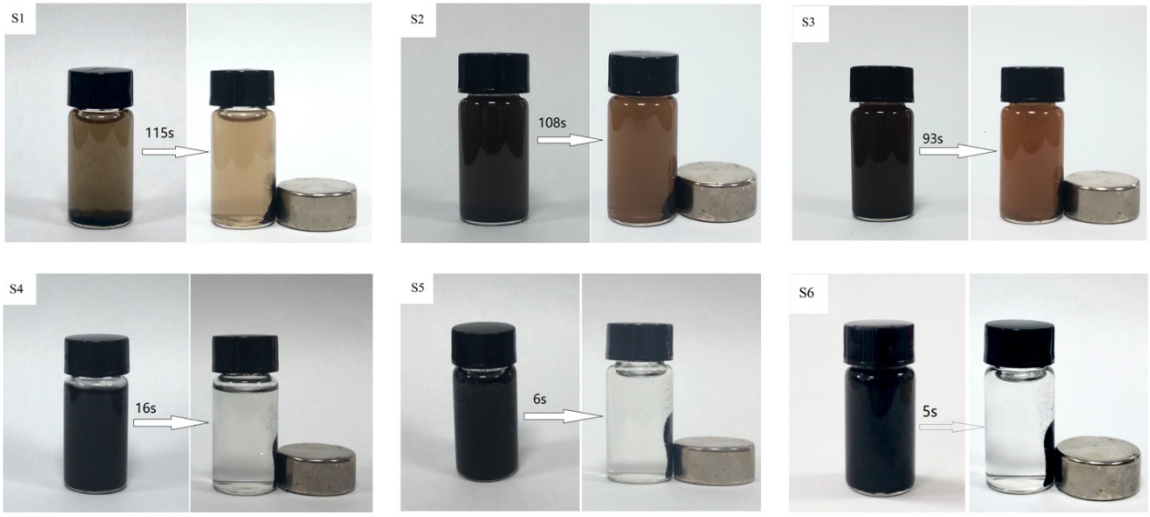

Figure 4. Dispersion degree of the samples (S1–S6) in ethanol solution and the magnetic response time of the samples after applied magnetic field were studied.

3.3. Adsorption Performance

Methylene blue dye is easily soluble in water and difficult to eliminate. Due to the small size of Fe_3O_4 particles, large specific surface area and high surface activity, it increases the chance of contact with the coloring agent. It can reach the adsorption equilibrium in a short time, and quickly reduce the chroma of wastewater.

It can be seen from Figure 5a that in the initial stage of adsorption, the adsorption capacity increased rapidly with the increase of time. When the adsorption reached equilibrium, the adsorption capacity tended to be constant. This is because in the initial stage of adsorption, there are many vacancies on the surface of the adsorbent, and adsorption occurs easily. As the adsorption continues, the vacancies on the surface of the adsorbent lessen, and the adsorption rate significantly declines until an equilibrium is reached. The illustration in Figure 5a shows the adsorption process of MB on Fe_3O_4 at different durations. The color of the MB solution was dark blue in the beginning, and it became light blue after 2 min of adsorption with the adsorbent. After 160 min, the solution is nearly colorless, the solid–liquid separation effect of Fe_3O_4 is obvious, and the solution is very clear. Figure 5b is the relationship between absorbance and methylene blue concentration curve, fitting a linear standard curve and standard curve equation, bringing the absorbance of the sample to be measured into the equation, so as to calculate the concentration to be measured.

Figure 5b shows that, as the mass of adsorbent increases, the removal effect of MB gradually increases. When the dosage of adsorbent is 200 mg, the removal effect of MB is the best. Figure 5d is the adsorption isotherm drawn based on the Langmuir model [5,7]. R^2 reaches 0.82, indicating that the adsorption of MB on Fe_3O_4 conforms to the law of Langmuir isotherm adsorption equation. Calculated from the equation, the maximum

adsorption capacity of the sample is 62.5 mg/g. The Langmuir isotherm equation can be expressed as:

$$\frac{1}{q_e} = \frac{1}{q_{max}} + \frac{1}{b \quad q_{max} \quad c_e}$$

wherein, C_e is the equilibrium concentration of the solution of MB dye, q_e is the adsorption amount of MB, q_{max} is theoretical MB maximum amount of adsorption, b is the adsorption constant.

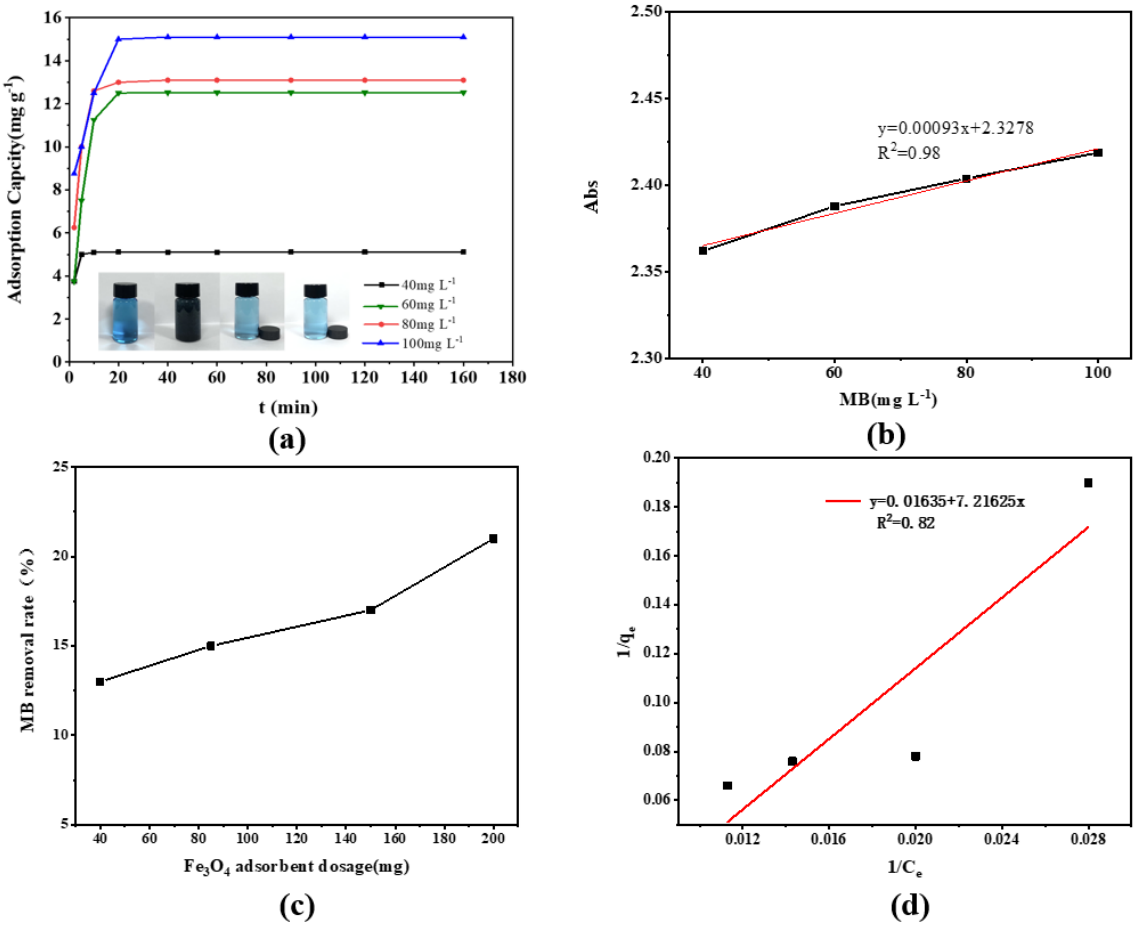

Figure 5. (**a**) Fe_3O_4 at different initial concentrations of methylene blue adsorption curve (The illustration shows the methylene blue solution, the solution after adding Fe_3O_4 magnetic adsorbent, the solution after 2 min of adsorption and 160 min after adsorption, from left to right); (**b**) the red line is the standard curve of the relationship between methylene blue concentration and absorbance; (**c**) the influence of the mass of adsorbent on the removal rate of MB; (**d**) the red line represents the Langmuir isotherm of Fe_3O_4.

The adsorption capacity of the Fe_3O_4 nano particles used in this experiment is greater than that of other adsorbents reported in the literature, such as Modified Bagasse Charcoal (q_{max} = 3.52 mg·g^{-1}) [32], modified biochar (q_{max} = 28.21 mg·g^{-1}) [33] and steel slag-montmorillonite composite adsorbent (q_{max} = 12.45 mg·g^{-1}) [34]. Most importantly, the magnetic adsorbent in this study can easily and quickly separate MB from the solution under the action of an external magnetic field, due to the high saturation magnetization of Fe_3O_4 nanoparticles, which simplifies the adsorption process and improves the adsorption efficiency. It is worth noting that, compared with Fe_3O_4 and based composite adsorbents prepared by other methods in previously reported works as summarized in Table 2, Fe_3O_4 prepared by one-step carbothermal reduction developed in this work has exhibited good magnetic properties, magnetic response, recyclability and better performance in wastewater treatment. In addition, the materials after the wastewater treatment experiment can be

recycled and reused just by facile ultrasonic cleaning to be discussed as following, which greatly reduces the total processing cost.

Table 2. Adsorption capacity of Fe_3O_4 adsorbents prepared by different methods.

Adsorbents	Synthesis Methods	Size (nm)	Ms (emu·g^{-1})	Adsorption Equilibrium Time	Adsorption Capacity (mg·g^{-1})	Ref.
Fe_3O_4	one-step reduction	~10	90.32	20 min	62.5	This work
	hydrothermal	13~23	67.77	20 min	40.1	[35]
	co-precipitation	6~8	74.3	-	34.9	[36]
	polyol	18~35	78.2	-	4.98	
	co-precipitation	15~30	65.33	40 min	53.1	[37]
GNS/Fe_3O_4 composite	-	200	42.9	30 min	43.82	[38]
ZrO_2/Fe_3O_4	one-step co-precipitation	1.18~4.56	12.7	72 h	29.5	[39]

3.4. Recycling of Fe_3O_4 Nanoparticles

The recyclability of Fe_3O_4 as an adsorbent is a common issue that deserves investigation in the pursuit of practical applications. In the recycling experiments, the Fe_3O_4 which adsorbed MB is separated from the solution with an external magnet, and then is re-dispersed into acidic methanol solution. After proper ultrasonic cleaning, Fe_3O_4 will be re-collected and dried for reuse to adsorb MB again. This process is repeated four times. As shown in Figure 6a, Fe_3O_4 magnetic powder after repeated use still retains its magnetic properties in aqueous solution. After detecting the absorbance of the supernatant after adsorption, it is concluded that Fe_3O_4 can adsorb MB many times, and the adsorption capacity is basically unchanged. It shows that the structure and magnetic properties of Fe_3O_4 are stable and that it could be reused.

In order to further study the adsorption mechanism of Fe_3O_4 NPs, XRD detection was performed on the Fe_3O_4 nanoparticles before and after adsorption. As shown in Figure 6b, seven identical characteristic peaks of Fe_3O_4 appeared before and after adsorption, and the interlayer spacing corresponding to the characteristic peaks of Fe_3O_4 before and after adsorption was almost unchanged, which indicates the adsorbate molecules did not enter or change the interior structures of the magnetic powder. Therefore, the adsorption of MB by magnetic Fe_3O_4 is the physical adsorption onto the outer surface by direct contact. Such physical adsorption is featured with low adsorption resistance between the adsorbate and the adsorbent, enabling Fe_3O_4 NPs to quickly adsorb MB molecules on its surface, when MB is in contact with Fe_3O_4 NPs. In addition, the physical adsorption benefits the separation between the adsorbate and the adsorbent during the reuse step. Therefore, such Fe_3O_4 NPs are endowed with both wastewater treatability and recyclability.

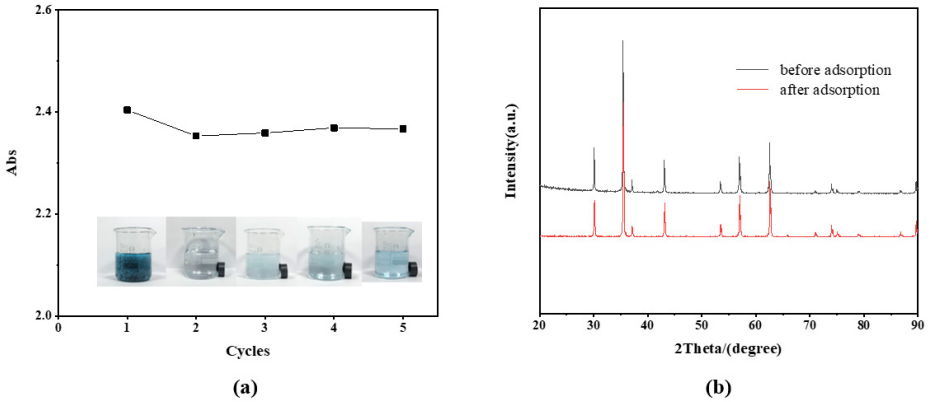

Figure 6. (**a**) Recyclability of Fe_3O_4 after MB adsorption. (The illustrations from left to right are the initial methylene blue solution after adding the magnetic Fe_3O_4 powder, and the water-dispersed magnetic powder which was attracted by the magnet after the first/second/third/fourth-cycle use and cleaning) (**b**) XRD of Fe_3O_4 before and after the adsorption of MB.

4. Conclusions

In summary, the purely-stoichiometric, monodisperse and small-sized (~10 nm) Fe_3O_4 nanoparticles were successfully synthesized by a one-step carbothermal method, in which the crystallinity of Fe_3O_4 nanoparticles was over 82%. Therefore, it has a high sensitivity magnetic response, a fast separation within 5 s under the action of an external magnetic field, and a high saturation magnetization of 90.32 emu/g. The performance of such Fe_3O_4 nanoparticles in the removal of methylene blue from aqueous solutions was studied in detail. The results show that they have a significant quick decolorization effect on methylene blue with a high adsorption capacity of 62.5 $mg \cdot g^{-1}$. The adsorption process conforms to the Langmuir adsorption isotherm which indicates that a single molecule adsorption is the most likely to occur. Importantly, Fe_3O_4 nanoparticles' quick dye adsorption capability is accompanied with their recyclability by separating the adsorbed molecules from them by just using ultrasonic cleaning. Considering the simplicity of the whole manufacturing and wide application of magnetic nanomaterials as adsorbents, this method is promising to effectively solve the traditional problem of poor magnetic response of Fe_3O_4 nanomaterials used in wastewater treatment.

Author Contributions: Conceptualization, P.H. and Z.Y.; Software, X.-y.W.; Validation, Q.-g.C., R.D., T.C., W.-c.J., X.-y.Z. and F.F.Y.; Writing—Original Draft Preparation, W.-c.J.; Writing—Review and Editing, W.-c.J. and S.E.S.; Supervision, K.-s.W. All authors have read and agreed to the published version of the manuscript.

Funding: This research was funded by the Natural Science Foundation of China (NSFC, 51404181); the Fok Ying Tung Education Foundation (171101); the Youth Innovation Team of Shaanxi Universities (2019-2022); the Top young talents project of "special support program for high level talents" in Shaanxi Province of China (2018-2023); the ANU Futures Scheme (Q4601024); and the Australian Research Council (DP190100295, LE190100014).

Institutional Review Board Statement: Not applicable.

Informed Consent Statement: Not applicable.

Data Availability Statement: Data is contained within the article. The data presented in this study can be seen in the content above.

Acknowledgments: This work was supported by the Natural Science Foundation of China (NSFC, 51404181); the Fok Ying Tung Education Foundation (171101); the Youth Innovation Team of Shaanxi Universities (2019-2022); the Top young talents project of "special support program for high level talents" in Shaanxi Province of China (2018-2023); the ANU Futures Scheme (Q4601024); and the Australian Research Council (DP190100295, LE190100014).

Conflicts of Interest: The authors declare no conflict of interest.

References

1. Zhao, C.; Liu, X.; Zhang, X.; Yan, H.; Qian, Z.; Li, X.; Ma, Z.; Han, Q.; Pei, C. A facile one-step method for preparation of Fe_3O_4/CS/INH nanoparticles as a targeted drug delivery for tuberculosis. *Mater. Sci. Eng. C* **2017**, *77*, 1182–1188. [CrossRef] [PubMed]
2. Mirabello, G.; Ianiro, A.; Bomans, P.H.H.; Yoda, T.; Arakaki, A.; Friedrich, H.; De With, G.; Sommerdijk, N. Crystallization by particle attachment is a colloidal assembly process. *Nat. Mater.* **2020**, *19*, 391–396. [CrossRef] [PubMed]
3. Cardoso, V.F.; Francesko, A.; Ribeiro, C.; Bañobre-López, M.; Martins, P.; Lanceros-Mendez, S. Advances in Magnetic Nanoparticles for Biomedical Applications. *Adv. Healthc. Mater.* **2018**, *7*, 1700845. [CrossRef]
4. Tadic, M.; Kralj, S.; Kopanja, L. Synthesis, particle shape characterization, magnetic properties and surface modification of superparamagnetic iron oxide nanochains. *Mater. Charact.* **2019**, *148*, 123–133. [CrossRef]
5. Yani, H.; Juan, X.; Qinqin, Z.; Chang, C.; Chuan, W. Facile synthesis of surface-functionalized magnetic nanocomposites for effectively selective adsorption of cationic dyes. *Nanoscale Res. Lett.* **2018**, *31*, 99.
6. Cursaru, L.M.; Piticescu, R.M.; Dragut, D.V.; Tudor, I.A.; Kuncser, V.; Iacob, N.; Stoiciu, F. The Influence of Synthesis Parameters on Structural and Magnetic Properties of Iron Oxide Nanomaterials. *Nanomaterials* **2020**, *10*, 85. [CrossRef]
7. Bai, L.; Li, Z.; Zhang, Y.; Wang, T.; Lu, R.; Zhou, W.; Gao, H.; Zhang, S. Synthesis of water-dispersible graphene-modified magnetic polypyrrole nanocomposite and its ability to efficiently adsorb methylene blue from aqueous solution. *Chem. Eng. J.* **2015**, *279*, 757–766. [CrossRef]

8. Brandl, F.; Bertrand, N.; Lima, E.M.; Langer, R. Nanoparticles with photoinduced precipitation for the extraction of pollutants from water and soil. *Nat. Commun.* **2015**, *6*, 7765. [CrossRef]
9. Mitra, S.; Sarkar, A.; Sen, S. Removal of chromium from industrial effluents using nanotechnology: A review. *Nanotechnol. Environ. Eng.* **2017**, *2*, 11. [CrossRef]
10. Shao, Y.; Zhou, L.; Bao, C.; Ma, J.; Liu, M.; Wang, F. Magnetic responsive metal–organic frameworks nanosphere with core–shell structure for highly efficient removal of methylene blue. *Chem. Eng. J.* **2016**, *283*, 1127–1136. [CrossRef]
11. Ranjithkumar, V.; Sangeetha, S.; Vairam, S. Synthesis of magnetic activated carbon/alpha-Fe_2O_3 nanocomposite and its application in the removal of acid yellow 17 dye from water. *J. Hazard. Mater.* **2014**, *273*, 127–135. [CrossRef] [PubMed]
12. Zhang, Q.; Wu, B.; Song, R.; Song, H.; Zhang, J.; Hu, X. Preparation, characterization and tribological properties of polyalphaolefin with magnetic reduced graphene oxide/Fe_3O_4. *Tribol. Int.* **2020**, *141*, 105952. [CrossRef]
13. Bi, H.; Yin, Z.; Cao, X.; Xie, X.; Tan, C.; Huang, X.; Chen, B.; Lu, X.; Sun, L.; Zhang, H. Twisted carbon fiber aerogels from raw cotton as sorbents for oils and organic solvents. *Adv. Mater.* **2013**, *25*, 5916–5921. [CrossRef] [PubMed]
14. Bi, H.; Huang, X.; Wu, X.; Cao, X.; Tan, C.; Yin, Z.; Lu, X.; Sun, L.; Zhang, H. Carbon micro belt aerogel prepared by waste paper: An efficient and recyclable sorbent for oils and organic solvents. *Small* **2014**, *10*, 3544. [CrossRef]
15. Uddin, N.; Zhang, H.; Du, Y.; Jia, G.; Wang, S.; Yin, Z. Structural-Phase Catalytic Redox Reactions in Energy and Environmental Applications. *Adv. Mater.* **2020**, *32*, 1905739. [CrossRef]
16. Ma, T.; Sun, S.; Fu, G.; Hall, J.W.; Ni, Y.; He, L.; Yi, J.; Zhao, N.; Du, Y.; Pei, T.; et al. Pollution exacerbates China's water scarcity and its regional inequality. *Nat. Commun.* **2020**, *11*, 650. [CrossRef]
17. Kinuthia, G.K.; Ngure, V.; Beti, D.; Lugalia, R.; Wangila, A.; Kamau, L. Levels of heavy metals in wastewater and soil samples from open drainage channels in Nairobi, Kenya: Community health implication. *Sci. Rep.* **2020**, 8434. [CrossRef]
18. Huang, Z.; Li, Y.; Chen, W.; Shi, J.; Zhang, N.; Wang, X.; Li, Z.; Gao, L.; Zhang, Y. Modified bentonite adsorption of organic pollutants of dye wastewater. *Mater. Chem. Phys.* **2017**, *202*, 266–276. [CrossRef]
19. Kuppusamy, S.; Jayaraman, N.; Jagannathan, M.; Kadarkarai, M.; Aruliah, R. Electrochemical decolorization and biodegradation of tannery effluent for reduction of chemical oxygen demand and hexavalent chromium. *J. Water Process Eng.* **2017**, *20*, 22–28. [CrossRef]
20. Pandey, S. A comprehensive review on recent developments in bentonite-based materials used as adsorbents for wastewater treatment. *J. Mol. Liq.* **2017**, *241*, 1091–1113. [CrossRef]
21. Chen, C.; Wang, J.; Liu, D.; Yang, C.; Liu, Y.; Ruoff, R.S.; Lei, W. Functionalized boron nitride membranes with ultrafast solvent transport performance for molecular separation. *Nat. Commun.* **2018**, *9*, 1902. [CrossRef] [PubMed]
22. Mustapha, S.; Tijani, J.O.; Ndamitso, M.M.; Abdulkareem, S.A.; Shuaib, D.T.; Mohammed, A.K.; Sumaila, A. The role of kaolin and kaolin/ZnO nanoadsorbents in adsorption studies for tannery wastewater treatment. *Sci. Rep.* **2020**, *10*, 13068. [CrossRef] [PubMed]
23. Makarchuk, O.V.; Dontsova, T.A.; Astrelin, I.M. Magnetic Nanocomposites as Efficient Sorption Materials for Removing Dyes from Aqueous Solutions. *Nanoscale Res. Lett.* **2016**, *11*, 161. [CrossRef] [PubMed]
24. Noreen, S.; Bhatti, H.; Zuber, M.; Zahid, M.; Asgher, M. Removal of actacid orange-RL dye using biocomposites: Modeling studies. *Pol. J. Environ. Stud.* **2017**, *26*, 2125–2134. [CrossRef]
25. Hu, P.; Chang, T.; Chen, W.-J.; Deng, J.; Li, S.-L.; Zuo, Y.-G.; Kang, L.; Yang, F.; Hostetter, M.; Volinsky, A.A. Temperature effects on magnetic properties of Fe_3O_4 nanoparticles synthesized by the sol-gel explosion-assisted method. *J. Alloy. Compd.* **2019**, *775*, 605–611. [CrossRef]
26. Ping, H.; Lu, K.; Jun, Y.; Fan, Y.; Kuaishe, W.; Jinjing, D.; Zhanlin, Y.; Weicheng, C.; DongXin, L. Synthesis of Fe Nanoparticles via One-Step Reduction Method. *Rare Met. Mat. Eng.* **2016**, *45*, 3112–3114. [CrossRef]
27. Hu, P.; Zhang, S.; Wang, H.; Pan, D.A.; Tian, J.; Tang, Z.; Volinsky, A.A. Heat treatment effects on Fe3O4 nanoparticles structure and magnetic properties prepared by carbothermal reduction. *J. Alloy. Compd.* **2011**, *509*, 2316–2319. [CrossRef]
28. Wang, H.; Hu, P.; Pan, D.A.; Tian, J.; Zhang, S.; Volinsky, A.A. Carbothermal reduction method for Fe_3O_4 powder synthesis. *J. Alloy. Compd.* **2010**, *502*, 338–340. [CrossRef]
29. Blanco-Andujar, C.; Walter, A.; Cotin, G.; Bordeianu, C.; Mertz, D.; Felder-Flesch, D.; Begin-Colin, S. Design of iron oxide-based nanoparticles for MRI and magnetic hyperthermia. *Nanomed. Nanotechnol.* **2016**, *11*, 1889–1910. [CrossRef]
30. Tadic, M.; Kralj, S.; Lalatonne, Y.; Motte, L. Iron oxide nanochains coated with silica: Synthesis, surface effects and magnetic properties. *Appl. Surf. Sci.* **2019**, *476*, 641–646. [CrossRef]
31. Venkatesha, N.; Poojar, P.; Qurishi, Y.; Geethanath, S.; Srivastava, C. Graphene oxide-Fe_3O_4 nanoparticle composite with high transverse proton relaxivity value for magnetic resonance imaging. *J. Appl. Phys.* **2015**, *117*, 4702–154709. [CrossRef]
32. Fujie, L.; Zhengda, L.; Xing, L.; Jiaying, L.; Zhenzhen, L.; Yayin, J. Adsorption of Cr(VI) on Modified Bagasse Charcoal. *Technol. Dev. Chem. Ind.* **2020**, *49*, 9.
33. Hafshejani, L.D.; Hooshmand, A.; Naseri, A.A.; Mohammadi, A.S.; Abbasi, F.; Bhatnagar, A. Removal of nitrate from aqueous solution by modified sugarcane bagasse biochar. *Ecol. Eng.* **2016**, *95*, 101–111. [CrossRef]
34. Tian, X.Z.; Jin, L.S.; Ying, B. Adsorption of Cd^{2+} from aqueous solution by steel slag-montmorillonite composite adsorbent. *Acta Sci. Circumst.* **2015**, *35*, 207–214.
35. Xing, Z.; Tang, B.; Chen, X.; Fu, F.; Zhang, Z.; Lu, Z. Adsorption mechanism of acid red 73 onto magnetic nanoparticles Fe3O4 from aqueous phase. *Acta Sci. Circumst.* **2014**, *4*, 2246–2255.

36. Shen, Y.F.; Tang, J.; Nie, Z.H.; Wang, Y.D.; Ren, Y.; Zuo, L. Tailoring size and structural distortion of Fe_3O_4 nanoparticles for the purification of contaminated water. *Bioresour. Technol.* **2009**, *100*, 4139–4146. [CrossRef]
37. Rajput, S.; Pittman, C.U.; Mohan, D. Magnetic magnetite (Fe_3O_4) nanoparticle synthesis and applications for lead (Pb^{2+}) and chromium (Cr^{6+}) removal from water. *J. Colloid Interface Sci.* **2016**, *468*, 334–346. [CrossRef]
38. Ai, L.; Zhang, C.; Chen, Z. Removal of methylene blue from aqueous solution by a solvothermal-synthesized graphene/magnetite composite. *J. Hazard. Mater.* **2011**, *192*, 1515–1524. [CrossRef]
39. Wang, J.; Shao, X.; Liu, J.; Zhang, Q.; Ma, J.; Tian, G. Insight into the effect of structural characteristics of magnetic ZrO2/Fe3O4 nanocomposites on phosphate removal in water. *Mater. Chem. Phys.* **2020**, *249*, 123024. [CrossRef]